Perturbation of Diminutive Solar Irradiance and Extreme Semiconductor Temperature on the Output Current and Voltage: The Translation of Electrical Characteristics into Thermal Char...

2 authors:

Stephen Ndubuisi Nnamchi
Kampala International University (KIU)
39 PUBLICATIONS   **127** CITATIONS

SEE PROFILE

Onyinyechi Adanma Nnamchi
Michael Okpara University of Agriculture, Umudike
14 PUBLICATIONS   **49** CITATIONS

SEE PROFILE

Some of the authors of this publication are also working on these related projects:

Development of hot spot arrestor View project

Design and fabrication of insulation testing rig View project

Journal of Solar Energy Research (JSER)

Journal homepage: www.jser.ut.ac.ir

JSER

Perturbation of Diminutive Solar Irradiance and Extreme Semiconductor Temperature on the Output Current and Voltage: The Translation of Electrical Characteristics into Thermal Characteristics

S. N. Nnamchi[1*a], O. A. Nnamchi[2]

[1.] *Department of Mechanical Engineering, Kampala International University, Ggaba Road, Kansanga, P.O.B 20000 Kampala, Uganda, stephen.nnamchi@kiu.ac.ug, ORCID: 0000-0002-6368-2913*
[2.] *Department of Agricultural Engineering and Bio Resources, Michael Okpara University of Agriculture, Umudike, Umuahia, Nigeria, onyxhoni@yahoo.com, ORCID: 0000-0003-4099-601X*

ARTICLE INFO

A B S T R A C T

Perturbation of diminutive solar irradiance and extreme semiconductor temperature on the responsive; output current and output voltage shows the stimulus effect of diminutive solar irradiance and extreme semiconductor temperature on the responsive. This could be adduced by carrying out direct and relative perturbation of the responsive with respect to diminutive solar irradiance and extreme semiconductor temperature. The upshot from the perturbation of output current and output voltage reveals that the output current is strongly influenced by the perturbation of diminutive solar irradiance whereas the output voltage is intensely influenced by the perturbation of extreme semiconductor temperature. Analytically, crystalline and thin film semiconductors proved to be rugged under the extreme semiconductor temperature and diminutive solar irradiance sequel to appreciable magnitude of their output current and output voltage gradients; 0.085060718 A/K, 0.044481542 V/K, 0.006285375 Am^2/W and 3.504405002 Vm^2/W, respectively. Furthermore, the relative perturbation of output current and output voltage gave rise to important thermal characteristics of the fluid surrounding the semiconductors investigated (crystalline; mono-c-Si and poly-c-Si, and thin films; copper indium dieseline and cadmium telluride); the internal conductance (convective and radiative heat transfer coefficients) and their corresponding thermal resistance (series and parallel) are the end products of perturbation rather than the complex classical correlation. These results provide a short cut and reliable means of establishing the thermal characteristics of fluid pocket surrounding the semiconductor, which are very useful for the performance analysis of the photovoltaic systems.
© 2019 Published by University of Tehran Press. All rights reserved.

1. Introduction

The performance of a photovoltaic module is jointly influenced by the solar irradiance, semiconductor temperature, and ambient conditions (air temperature and wind speed). The magnitude of the output current and voltage generated from a photovoltaic module partly depends on the response of the equivalent ciruit parameters to the stimuli (solar irradiance and semiconductor temperature). Under normal operating condition, the solar irradiance positively impact on all the photovoltaic

parameters (photon current, diode saturation current, ideality factor, series and shunt resistance) which engenders high output power sequel to simultaneous increase in the output current and output voltage. increase in the output current and output voltage. However, the semiconductor temperature negatively impacts on some of these responsive parameters (diode saturation current, ideality and shunt resistance) such that the output voltage is decreased and output current slightly increased, which leads to a reduction in the output power [1].

---

[a]* Corresponding author at: Department of Mechanical Engineering, KIU, Kampala, Uganda.
E-mail addresses: stephen.nnamchi@kiu.ac.ug, nnasteve@yahoo.com, +256701966149.

Principally, an isotropic or pure semiconductor in equilibrium condition has balanced number of intrinsic charge carriers (electrons, n = holes, p). Under the effect of diffusion or electric field, the electrons wholly diffuse or drift to the conductor band (electron host) whereas the holes entirely diffuse or drift to the valence band (hole host). Conversely, an anisotropic or doped semiconductor in non-equilibrium condition has either surplus or deficit of charge carriers corresponding to recombination and generation of charge carriers [1], [2], [3]. The recombination of charge carriers is favoured by abnormal semiconductor temperature, which increases the number of charge carriers above the intrinsic charge carriers whereas the generation of charge carriers is favoured by normal semiconductor temperature, which reduces the number of charge carriers below the intrinsic charge carriers [1]. However, thermalisation emanates as a result of photon light energy much greater than the spectral absorption band of the semiconductor (energy gap), the excess energy heats up the semiconductor lattice and impairs the efficiency of the photovoltaic module [4].

Inexorably, solar irradiance in excess of energy gap of the semiconductor ends up raising the semiconductor temperature which promotes recombination of charge carriers but solar irradiance proportionate to the energy gap of semicondutor supports generation of charge carriers [5]. The recombination of charge carriers impairs the conversion of solar irradiance to electrial power whereas generation of charge carrier enhances the conversion of solar irradiance to electrical power. Salim et al. [6] is of opinion that increase in solar irradiance is associated with an increase in output power of a photovoltaic module provided that the semiconductor material has energy gap to accommodate the available solar irradiance. However, the output voltage decreases with increase in semiconductor temperature, culminating in low efficiency of the semiconductor in converting solar irradiance to electrical power [7].

Considerably, the output current versus output voltage curves portray that there is a prevalent linear relationship between the solar irradiance and output current, and nonlinear or logarithm relationship between the solar irradiance and output voltage, which reflects their susceptibility to solar irradiance. Contrarily, an increase in semiconductor temperature significantly decreases the voltage while the output current is slight increased, which explains their sensitivity to the semiconductor temperature.

Thus, a drop in the efficiency of photovoltaic module is succinctly dissociated to the solar irradiance and unequivocally associated to the semiconductor temperature [8].

Similarly, there is an inverse or indirect relationship between the ambient air temperature and efficiency of a photovoltaic module. Thus, high ambient temperature does not support effective cooling of the semiconductors. However, low ambient temperature coupled with a windy condition enhances the performance of the semiconductors while high ambient temperature on a calm condition hampers the efficiency of the semiconductors [9].

Pertinently, Nnamchi et al. [10] have carried out extensive studies on the stimuli; solar irradiance and semiconductor temperature. They were able to develop nonlinear monthly thermal input models of the stimulus (solar irradiance) as a function of time and that of semiconductor temperature as a function of solar irradiancce, ambient temperature and wind speed. In the absence of pyranometer, these models are useful for the prediction of solar irradiance and semiconductor temperature.

Moreover, Nnamchi et al. [1] and Cubas et al. [11] proposed photovoltaic parameter modification for the five parameter equivalent circuit model sequel to the development of solar irradiance coefficients alongside with the semiconductor temperature coefficients; the classical model of photon current, diode reverse current, ideality factor, series resistance and shunt resistance has been modified such that the influence of both solar irradiance and semiconductor temperature could be accounted on the stimuli (diminutive solar irradiance, G and extreme semiconductor temperature, T). This modification has opened a window for performing perturbation of solar irradance and semiconductor temperature on the photovoltaic parameters aforementioned, the output current and output voltage which comprise the responsive or receptive.

Upon this adventure, the present work will explore the behaviour of photovoltaic module under the awakward conditions; the diminutive solar iradiance and extreme semiconductor temperature in order to fathom the influence of the stimuli on the responsive. The perturbation will unveil the response of the output current and output voltage to the stimuli, and equally establish the thermal characteristics (the internal conductance and resistance) of air pocket within the photovoltaic module.

2. Materials and Methods

The research employs mechanistic models (ordinary and partial differential equations) in setting up perturbation models. The perturbed model result (numerical value) is employed in determining the response of the photovoltaic parameters, the output current and output voltage to the stimuli (solar irradiance and semiconductor temperature). Moreover, the mechanistic models on the output current and output voltage will be translated into non-mechanistic or regression models to obtain thermal regression models (the internal conductance and resistance) around the semiconductor materials (mono crystalline silicon, poly crystalline silicon, copper indium diselenide and cadmium telluride) as a function of semiconductor temperature.

2.1 The equivalent circuit model

The equivalent circuit model simply demonstrates how photon current (I_{ph}) splits into diode current (I_D), shunt or parallel current (I_P) and the output current (I); and the applied output voltage (V) in Figure 1.
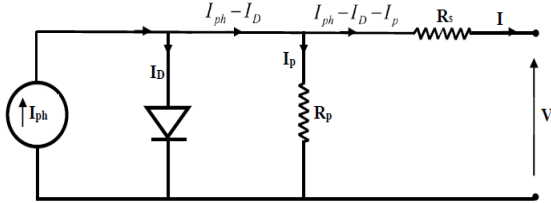

Figure 1. Diagrammatic representation of equivalent circuit model

According to Kirchhoff's nodal law, the source or photon current travels down the circuit to produce the diode current, shunt current, output current and output voltage [1], [11], [12], [13] as follows:

$$I = I_{ph} - I_D - I_p = I_{ph} - I_o\left(e^{\left(\frac{V+I R_s}{A V_T}\right)} - 1\right) - \frac{V + I R_s}{R_p} \quad (1)$$

whereas, V_T is the thermal voltage developed in the semiconductor which is expressed in Equation (2) as

$$V_T = \frac{n_s K_B T}{q_c}; \ n_s \leq 36 \ \text{or} \ V_T = \frac{K_B T}{q_c}; \ n_s > 36 \quad (2)$$

where n_s = number of cells in series (-), K_B = Boltzmann constant (J/K), T = nominal operating temperature (K) of the semiconductor and q_c = electron charge (C).

Strategically, the modified parameters [14], [15], [16] are appropriate for the perturbation of solar irradiance and semiconductor temperature with the availability of

solar irradiance coefficient (γ) and semiconductor temperature coefficient (κ).

The modified photon current, I_{ph} [1], [17] is written in Equation (3) as follows:

$$
\begin{aligned}
I_{ph} &= I_{ph\_0}\left(1 + \kappa_i\,\Delta T + \sqrt{\gamma_i G}\right)\frac{G}{G_0} \\
&= I_{ph\_0}\left(1 + \kappa_i(T - T_0) + \sqrt{\gamma_i G}\right)\frac{G}{G_0}
\end{aligned}
\quad (3)
$$

The thermal modification of standard test condition (STC) parameters at short circuit, maximum power point and open circuit is found in [11], [18]; the modification accounts for change in semiconductor temperature alone but the present work systematically considers the influence of both solar irradiance and semiconductor temperature in formulating diode reverse saturation current, I_0 [1], [11], [18] in Equation (4)

$$I_0 = I_{0\_0}\left(1 + \kappa_i\Delta T + \sqrt{\gamma_i G}\right)\left(\frac{T_0}{T}\right)^3 \exp\left(\frac{q_c E_g}{A K_B}\left(\frac{1}{T_0} - \frac{1}{T}\right)\right) \quad (4)$$

The modified ideality factor, A [1], [11], [17], [18] is well furnished in Equation (5)

$$A = \frac{I_{mpp} V_{oc}}{I_{sc} V_{mpp}}\left(1 + \kappa_i\Delta T + \sqrt{\gamma_i G}\right) = A_0\left(1 + \kappa_i\Delta T + \sqrt{\gamma_i G}\right) \quad (5)$$

The modified series resistance, R_s [1], [11], [17], [18] is given in Equation (6)

$$R_s = \frac{n_p}{n_s}\left(1 - \frac{I_{mpp}}{I_{sc}}\frac{V_{mpp}}{V_{oc}}\right)\left(\frac{V_{oc}\left(1 + \kappa_v\Delta T + \sqrt{\gamma_v G}\right)}{I_{sc}\left(1 + \kappa_i\Delta T + \sqrt{\gamma_i G}\right)} - \frac{V_{mpp}\left(1 + \kappa_v\Delta T + \sqrt{\gamma_v G}\right)}{I_{mpp}\left(1 + \kappa_i\Delta T + \sqrt{\gamma_i G}\right)}\right) + \zeta \quad (6)$$

where ζ is an adjustment factor.

Similarly, the modified parallel resistance, R_p [1], [11], [17], [18] is clearly defined in Equation (7)

$$R_p = \frac{V_{mpp}\left(1 + \kappa_v\Delta T + \sqrt{\gamma_v G}\right) + I_{mpp}\left(1 + \kappa_i\Delta T + \sqrt{\gamma_i G}\right)\left(\frac{G}{G_0}\right)R_s}{I_{ph} - I_o\left(e^{\frac{V_{mpp}\left(1+\kappa_v\Delta T+\sqrt{\gamma_v G}\right)+I_{mpp}\left(1+\kappa_i\Delta T+\sqrt{\gamma_i G}\right)\left(\frac{G}{G_0}\right)R_s}{A V_T}} - 1\right) - I_{mpp}\left(1 + \kappa_i\Delta T + \sqrt{\gamma_i G}\right)\left(\frac{G}{G_0}\right)} \quad (7)$$

$$> R_{p,min};$$

where the modified minimum parallel resistance, $R_{P,min}$ [1], [11], [17], [18] at nominal operating condition is explicitly given in Equation (8)

$$R_{p,\min} = \cfrac{V_{mpp}\left(1 + \kappa_v \Delta T + \sqrt{\gamma_v G}\right)}{\left(I_{sc}\left(1 + \kappa_i \Delta T + \sqrt{\gamma_i G}\right) - I_{mpp}\left(1 + \kappa_i \Delta T + \sqrt{\gamma_i G}\right)\right)\dfrac{G}{G_0}} - \cfrac{V_{oc}\left(1 + \kappa_v \Delta T + \sqrt{\gamma_v G}\right) - V_{mpp}\left(1 + \kappa_v \Delta T + \sqrt{\gamma_v G}\right)}{I_{mpp}\left(1 + \kappa_i \Delta T + \sqrt{\gamma_i G}\right)\dfrac{G}{G_0}} \tag{8}$$

2.2 Perturbation of semiconductor temperature and solar irradiance

The perturbation of semiconductor temperature and solar irradiance is centered on the output current and output voltage.

The perturbation of the output current with respect to (wrt) semiconductor temperature is presented in Equation (9) as follows:

$$\frac{dI}{dT} = \frac{\partial I}{\partial I_{ph}}\frac{\partial I_{ph}}{\partial T} + \frac{\partial I}{\partial I_0}\frac{\partial I_0}{\partial T} + \frac{\partial I}{\partial A}\frac{\partial A}{\partial T} + \frac{\partial I}{\partial R_s}\frac{\partial R_s}{\partial T} + \frac{\partial I}{\partial R_p}\frac{\partial R_p}{\partial T} \tag{9}$$

The derivative of the output current, I wrt photon current, I_{ph} in Equation (1) is expressed in Equation (10a)

$$\frac{\partial I}{\partial I_{ph}} = \frac{1}{1 + \dfrac{I_0 R_s}{A V_T}\exp\left(\dfrac{V + I R_s}{A V_T}\right) + \dfrac{R_s}{R_p}} \tag{10a}$$

and $\dfrac{\partial I_{ph}}{\partial T}$ in Equation (10b) is specifically given [1] as

$$\frac{\partial I_{ph}}{\partial T} = \kappa_i I_{ph0\_0}\frac{G}{G_0} = \frac{\kappa_i I_{ph}}{1 + \kappa_i \Delta T + \sqrt{\gamma_i G}} \tag{10b}$$

The derivative of the output current, I wrt diode reverse or saturation current, I_0 in Equation (1) is explicitly given in Equation (11a)

$$\frac{\partial I}{\partial I_0} = \frac{-\left(\exp\left(\dfrac{V + I R_s}{A V_T}\right) - 1\right)}{1 + \dfrac{I_0 R_s}{A V_T}\exp\left(\dfrac{V + I R_s}{A V_T}\right) + \dfrac{R_s}{R_p}} \tag{11a}$$

whereas $\dfrac{\partial I_0}{\partial T}$ in Equation (11b) is explicitly given [1] as

$$\frac{\partial I_0}{\partial T} = I_0\left(\frac{\kappa_i}{1 + \kappa_i \Delta T + \sqrt{\gamma_i G}} - \frac{3}{T} + \frac{q_c E_g}{A K_B}\left(\frac{1}{T^2} - \frac{1}{A}\left(\frac{1}{T_0} - \frac{1}{T}\right)\frac{\partial A}{\partial T}\right)\right); \tag{11b}$$

The derivative of the output current, I wrt ideality factor, A in Equation (1) is stated in Equation (12a)

$$\frac{\partial I}{\partial A} = \frac{\left(\dfrac{I_0\left(V + I R_s\right)}{A^2 V_T}\exp\left(\dfrac{V + I R_s}{A V_T}\right)\right)}{1 + \dfrac{I_0 R_s}{A V_T}\exp\left(\dfrac{V + I R_s}{A V_T}\right) + \dfrac{R_s}{R_p}} \tag{12a}$$

while $\dfrac{\partial A}{\partial T}$ in Equation (12b) is clearly given [1] as

$$\frac{\partial A}{\partial T} = k_i A_0 = \frac{\kappa_i A}{1 + \kappa_i \Delta T + \sqrt{\gamma_i G}} \tag{12b}$$

The derivative of the output current, I wrt series resistance, R_s in Equation (1) is articulated in Equation (13a)

$$\frac{\partial I}{\partial R_s} = \frac{-I\left(\dfrac{I_0}{A V_T}\exp\left(\dfrac{V + I R_s}{A V_T}\right) + \dfrac{1}{R_p}\right)}{1 + \dfrac{I_0 R_s}{A V_T}\exp\left(\dfrac{V + I R_s}{A V_T}\right) + \dfrac{R_s}{R_p}} \tag{13a}$$

but $\dfrac{\partial R_s}{\partial T}$ in Equation (12b) is unambiguously given [1] as

$$\frac{\partial R_s}{\partial T} = R_{s\_0}\left(\frac{\dfrac{\kappa_v}{1 + \kappa_i \Delta T + \sqrt{\gamma_i G}}}{} - \frac{\kappa_i\left(1 + \kappa_v \Delta T + \sqrt{\gamma_v G}\right)}{\left(1 + \kappa_i \Delta T + \sqrt{\gamma_i G}\right)^2}\right) \tag{13b}$$

The derivative of the output current, I wrt parallel or shunt resistance, R_p in Equation (1) is derived in Equation (14a)

$$\frac{\partial I}{\partial R_p} = \frac{\left(V + I R_s\right)/R_p^2}{1 + \dfrac{I_0 R_s}{A V_T}\exp\left(\dfrac{V + I R_s}{A V_T}\right) + \dfrac{R_s}{R_p}} \tag{14a}$$

and

$$\frac{\partial R_p}{\partial T} = \frac{\left(a\dfrac{\partial b}{\partial T} - b\dfrac{\partial a}{\partial T}\right)}{b^2} \tag{14b}$$

where

$$a = V_{mpp}\left(1 + \kappa_v \Delta T + \sqrt{\gamma_v G}\right) + I_{mpp}\left(1 + \kappa_i \Delta T + \sqrt{\gamma_i G}\right)\left(G/G_0\right)R_s \tag{14c}$$

$$b = I_{ph} - I_0 \left(e^{\frac{a}{AV_T}} - 1 \right)$$
$$- I_{mpp} \left(1 + \kappa_i \Delta T + \sqrt{\gamma_i G} \right) (G/G_0) \tag{14d}$$

$$\frac{\partial a}{\partial T} = \kappa_v V_{mpp} + \kappa_i I_{mpp} (G/G_0) R_s$$
$$+ I_{mpp} \left(1 + \kappa_i \Delta T + \sqrt{\gamma_i G} \right) (G/G_0) \frac{\partial R_s}{\partial T} \tag{14e}$$

where the partial derivative $\dfrac{\partial R_s}{\partial T}$ is defined in Equation (13b),

$$\frac{\partial b}{\partial T} = \frac{\partial I_{ph}}{\partial T} - \frac{\partial I_o}{\partial T} \left(e^{\frac{a}{AV_T}} - 1 \right)$$
$$- I_0 \left(\frac{AV_T \frac{\partial a}{\partial T} - aA \frac{\partial V_T}{\partial T} - aV_T \frac{\partial A}{\partial T}}{A^2 V_T^2} \right) \left(e^{\frac{a}{AV_T}} \right) \tag{14f}$$
$$- \kappa_i I_{mpp} (G/G_0)$$

where the partial derivatives; $\dfrac{\partial I_{ph}}{\partial T}$, $\dfrac{\partial I_O}{\partial T}$, $\dfrac{\partial A}{\partial T}$, $\dfrac{\partial a}{\partial T}$

and $\dfrac{\partial V_T}{\partial T}$ are defined in Equations (10b), (11b), (12b), (14e) and (2), respectively.

The perturbation of the output voltage wrt semiconductor temperature is presented in Equation (15) as follows:

$$\frac{dV}{dT} = \frac{\partial V}{\partial I_{ph}} \frac{\partial I_{ph}}{\partial T} + \frac{\partial V}{\partial I_0} \frac{\partial I_0}{\partial T} + \frac{\partial V}{\partial A} \frac{\partial A}{\partial T} + \frac{\partial V}{\partial R_s} \frac{\partial R_s}{\partial T}$$
$$+ \frac{\partial V}{\partial R_p} \frac{\partial R_p}{\partial T} \tag{15}$$

where the derivatives; $\dfrac{\partial I_{ph}}{\partial T}$, $\dfrac{\partial I_0}{\partial T}$, $\dfrac{\partial A}{\partial T}$, $\dfrac{\partial R_s}{\partial T}$ and $\dfrac{\partial R_p}{\partial T}$

are defined in Equations (10b) - (14b), respectively.

The derivative of the output voltage, V wrt photon current, I_{ph} in Equation (1) is expressed in Equation (16)

$$\frac{\partial V}{\partial I_{ph}} = \frac{1}{\dfrac{I_0}{AV_T} \exp\left(\dfrac{V + IR_s}{AV_T} \right) + \dfrac{1}{R_p}} \tag{16}$$

The derivative of the output voltage, V wrt diode reverse or saturation current, I_0 in Equation (1) is given in Equation (17)

$$\frac{\partial V}{\partial I_0} = \frac{-\left(\exp\left(\dfrac{V + IR_s}{AV_T} \right) - 1 \right)}{\dfrac{I_0}{AV_T} \exp\left(\dfrac{V + IR_s}{AV_T} \right) + \dfrac{1}{R_p}} \tag{17}$$

The derivative of the output voltage, V wrt ideality factor, A in Equation (1) is stated in Equation (18)

$$\frac{\partial V}{\partial A} = \frac{\left(\dfrac{I_0 (V + IR_s)}{A^2 V_T} \exp\left(\dfrac{V + IR_s}{AV_T} \right) \right)}{\dfrac{I_0}{AV_T} \exp\left(\dfrac{V + IR_s}{AV_T} \right) + \dfrac{1}{R_p}} \tag{18}$$

The derivative of the output voltage, V wrt series resistance, R_s in Equation (1) is articulated in Equation (19)

$$\frac{\partial V}{\partial R_s} = \frac{-I \left(\dfrac{I_0}{AV_T} \exp\left(\dfrac{V + IR_s}{AV_T} \right) + \dfrac{1}{R_p} \right)}{\dfrac{I_0}{AV_T} \exp\left(\dfrac{V + IR_s}{AV_T} \right) + \dfrac{1}{R_p}} \tag{19}$$

The derivative of the output voltage, V wrt parallel or shunt resistance, R_p in Equation (1) is derived in Equation (20)

$$\frac{\partial V}{\partial R_p} = \frac{(V + IR_s)/R_p^2}{\dfrac{I_0}{AV_T} \exp\left(\dfrac{V + IR_s}{AV_T} \right) + \dfrac{1}{R_p}} \tag{20}$$

Similarly, the perturbation of the output current wrt semiconductor temperature is presented in Equation (21) as follows:

$$\frac{dI}{dG} = \frac{\partial I}{\partial I_{ph}} \frac{\partial I_{ph}}{\partial G} + \frac{\partial I}{\partial I_0} \frac{\partial I_0}{\partial G} + \frac{\partial I}{\partial A} \frac{\partial A}{\partial G} + \frac{\partial I}{\partial R_s} \frac{\partial R_s}{\partial G}$$
$$+ \frac{\partial I}{\partial R_p} \frac{\partial R_p}{\partial G} \tag{21}$$

where the derivatives; $\dfrac{\partial I_{ph}}{\partial G}$, $\dfrac{\partial I_0}{\partial G}$, $\dfrac{\partial A}{\partial G}$, $\dfrac{\partial R_s}{\partial G}$, and

$\dfrac{\partial R_p}{\partial G}$ in Equations (21a) – (21e) respectively are defined in [1] as

$$\frac{\partial I_{ph}}{\partial G} = I_{ph} \left(\frac{0.5 \gamma_i (\gamma_i G)^{-0.5}}{1 + \kappa_i \Delta T + \sqrt{\gamma_i G}} + \frac{1}{G} \right) \tag{21a}$$

whereas

$$\frac{\partial I_0}{\partial G} = \frac{0.5 \gamma_i (\gamma_i G)^{-0.5} I_0}{1 + \kappa_i \Delta T + \sqrt{\gamma_i G}} \tag{21b}$$

while

$$\frac{\partial A}{\partial G} = 0.5\gamma_i(\gamma_i G)^{-0.5}A_0 = \frac{0.5\gamma_i(\gamma_i G)^{-0.5}A}{1+\kappa_i\Delta T + \sqrt{\gamma_i G}} \qquad (21c)$$

while

$$\frac{\partial R_s}{\partial G} = 0.5R_s\,_{-0}\left(\begin{array}{c}\dfrac{\dfrac{\gamma_v(\gamma_v G)^{-0.5}}{1+\kappa_v\Delta T+\sqrt{\gamma_v G}}}{\ } \\ -\dfrac{\gamma_i(\gamma_i G)^{-0.5}\left(1+\kappa_v\Delta T+\sqrt{\gamma_v G}\right)}{\left(1+\kappa_i\Delta T+\sqrt{\gamma_i G}\right)^2}\end{array}\right) \qquad (21d)$$

and

$$\frac{\partial R_p}{\partial G} = \frac{\left(b\dfrac{\partial a}{\partial G} - a\dfrac{\partial b}{\partial G}\right)}{b^2} \qquad (21e)$$

where

$$\begin{aligned}\frac{\partial a}{\partial G} &= 0.5\gamma_v(\gamma_v G)^{-0.5}V_{mpp} + 0.5\gamma_i(\gamma_i G)^{-0.5}I_{mpp}(G/G_0)R_s \\ &+ I_{mpp}\left(1+\kappa_i\Delta T+\sqrt{\gamma_i G}\right)(R_s/G_0) \\ &+ I_{mpp}\left(1+\kappa_i\Delta T+\sqrt{\gamma_i G}\right)(G/G_0)\frac{\partial R_s}{\partial G}\end{aligned} \qquad (21f)$$

where the partial derivative $\dfrac{\partial R_s}{\partial G}$ is expressed in Equation (21d), and

$$\begin{aligned}\frac{\partial b}{\partial G} &= \frac{\partial I_{ph}}{\partial G} - \frac{\partial I_0}{\partial G}\left(e^{\frac{a}{AV_T}} - 1\right) \\ &- \frac{I_0\left(AV_T\dfrac{\partial a}{\partial G} - aV_T\dfrac{\partial A}{\partial G}\right)}{A^2 V_T^2}\left(e^{\frac{a}{AV_T}}\right) \\ &- 0.5\gamma_i(\gamma_i G)^{-0.5}I_{mpp}(G/G_0) \\ &- I_{mpp}\left(1+\kappa_i\Delta T+\sqrt{\gamma_i G}\right)(1/G_0)\end{aligned} \qquad (21g)$$

where the partial derivatives; $\dfrac{\partial I_{ph}}{\partial G}$, $\dfrac{\partial I_o}{\partial G}$, $\dfrac{\partial A}{\partial G}$ and $\dfrac{\partial a}{\partial G}$ are written in Equations (21b) – (21c), (21f), respectively.

The perturbation of the output voltage wrt semiconductor temperature is given in Equation (22)

$$\begin{aligned}\frac{dV}{dG} &= \frac{\partial V}{\partial I_{ph}}\frac{\partial I_{ph}}{\partial G} + \frac{\partial V}{\partial I_0}\frac{\partial I_0}{\partial G} + \frac{\partial V}{\partial A}\frac{\partial A}{\partial G} + \frac{\partial V}{\partial R_s}\frac{\partial R_s}{\partial G} \\ &+ \frac{\partial V}{\partial R_p}\frac{\partial R_p}{\partial G}\end{aligned} \qquad (22)$$

where the derivatives; $\dfrac{\partial I_{ph}}{\partial G}$, $\dfrac{\partial I_0}{\partial G}$, $\dfrac{\partial A}{\partial G}$, $\dfrac{\partial R_s}{\partial G}$ and $\dfrac{\partial R_p}{\partial G}$ are defined in Equations (21b) – (21e),

respectively; $\dfrac{\partial V}{\partial I_{ph}}$, $\dfrac{\partial V}{\partial I_0}$, $\dfrac{\partial V}{\partial A}$, $\dfrac{\partial V}{\partial R_s}$ and $\dfrac{\partial V}{\partial R_p}$ are given in Equations (16) – (20), respectively.

Table 1 provides the summary of perturbation of semiconductor temperature and solar irradiance.

The thermal conductance in Equation (23) is derived by the relative perturbation of I wrt to G and T

$$\tau\alpha(1-\eta)\frac{G^2}{T^2}\frac{dT}{dG}\bigg|_I = \tau\alpha(1-\eta)\frac{G^2}{T^2}\left(\frac{dI/dG}{dI/dT}\right) = h_r \qquad (23)$$

is equivalent to parallel or radiative conductance, (W/m²K); and thermal resistance in Equation (24) is obtained by the relative perturbation of I wrt to G and T

$$\frac{1}{\tau\alpha(1-\eta)}\frac{T^2}{G^2}\frac{dG}{dT}\bigg|_I = \frac{1}{\tau\alpha(1-\eta)}\frac{T^2}{G^2}\left(\frac{dI/dT}{dI/dG}\right) = R_r \qquad (24)$$

is equivalent to parallel or radiative resistance, $R_r = 1/h_r$ (m²K/W); and thermal conductance in Equation (25) is gotten by the relative perturbation of V wrt to G and T

$$\tau\alpha(1-\eta)\frac{G^2}{T^2}\frac{dT}{dG}\bigg|_V = \tau\alpha(1-\eta)\frac{G^2}{T^2}\left(\frac{dV/dG}{dV/dT}\right) = h_{conv} \qquad (25)$$

is equivalent to series or convective conductance, h_{conv} (W/m²K); and thermal resistance in Equation (26) established by the perturbation of V wrt to G and T

$$\frac{1}{\tau\alpha(1-\eta)}\frac{T^2}{G^2}\frac{dG}{dT}\bigg|_V = \frac{1}{\tau\alpha(1-\eta)}\frac{T^2}{G^2}\left(\frac{dV/dT}{dV/dG}\right) = R_{conv} \qquad (26)$$

is equivalent to series or convective resistance, $R_{conv} = 1/h_{conv}$ (m²K/W), where $\tau\alpha$ is the product of transmissivity-absorptivity, η is the efficiency of the semiconductor. Combining Equations (23) and (25) yields the effective thermal conductance (internal heat transfer coefficient), $h_{eff}\left(W/m^2K\right)$ in Equation (27)

$$h_{eff} = h_{conv} + h_r \qquad (27)$$

whereas adding Equations (24) and (25) gives the effective thermal resistance, $R_{eff}\left(m^2K/W\right)$ in Equation (28)

$$R_{eff} = \frac{(R_{conv}R_r)}{R_{conv} + R_r} \qquad (28)$$

According to Hammami et al. [19] in Nnamchi et al. [20] the convective heat transfer coefficient, h_{conv}

between the glass and semiconductor is given by classical correlation in Equation (29) as follows:

$$h_{conv} \approx \frac{k}{D_h}\left\{0.825 + \frac{0.387 Ra_{pv-glass}^{1/6}}{\left[1+\left(0.492/\mathrm{Pr}\right)^{9/16}\right]^{8/27}}\right\}^2$$

$$for \; 10^{-1} < Ra_{pv-glass} < 10^{12},$$

$$Ra_{pv-glass} = \frac{D_h^3 \rho^2 \beta \; cp \left(g \cos\varphi\right)\left(T_{pv} - T_{glass}\right)}{\mu k}, \qquad (29)$$

$$\mathrm{Pr} = \frac{\mu cp}{k}, \; \beta = \frac{2}{T_{pv} + T_{glass}};$$

$$T_{glass} = 0.9605 T_{pv} + 6.3505; \; \varphi \approx 0.35^o$$

where $k\left(W/mK\right)$ is the thermal conductivity of air, $D_h\left(m\right)$ is the equivalent hydraulic diameter between the glass and semiconductor, $Ra\left(-\right)$ is Rayleigh dimensionless number, $\mathrm{Pr}\left(-\right)$ is Prandtl dimensionless number, $\rho\left(kg/m^3\right)$ air density, $\beta\left(1/K\right)$ is temperature coefficient, $cp\left(kJ/kgK\right)$ is air specific heat capacity, $g\left(m/s^2\right)$ is gravitational constant, φ is the slope angle (degree,^{o}) of the module, $\mu\left(kg/ms\right)$ is air viscosity, $T\left(K\right)$ is temperature. Air temperature is considered to be average temperature between the glass and semiconductor (PV), ω (m) is the width of the module and δ (m) is the thickness of the module or semiconductor.

Table 1. Summary of perturbation of semiconductor temperature and solar irradiance

S#	Output variable	Differential (perturbation) operator	
		d/dT	d/dG
1.	I (Ampere)	$\dfrac{dI}{dT}$ (Equation (9))	$\dfrac{dI}{dG}$ (Equation (21))
2.	V (Volt)	$\dfrac{dV}{dT}$ (Equation (15))	$\dfrac{dV}{dG}$ (Equation (22))

2.3 Input data

The input constants and variables are expressed in Tables 2–5 [1]. The electrical characteristics of the crystalline silicon and thin-film photovoltaic semiconductors in Table 2, respectively were obtained from the manufacturer specification sheet [21], [22], [23], [24], [25]. Table 3 summaries the temperature and solar irradiance coefficients for the different semiconductors and Table 4 contains the feasible values of the photovoltaic parameters. Also, Table 5 presents the thermophysical properties of the air pocket surrounding the semiconductor.

3. Results & Discussion

The results are systematically presented in Section (3.1) whereas Section (3.2) features the comprehensive discussion of the results.

3.1 Presentation of results

Summarily, Tables 6 and 7 present the results of perturbation of the responsive (I and V) with respect to extreme semiconductor temperature (T) and diminutive solar irradiance (G), respectively. Subsequently, Figures 2 – 4 portray the outcome of perturbation of the output current and output voltage, which yielded two important thermal characteristics of the fluid pocket surrounding the semiconductors (mono-c-Si, poly-c-Silicon, CIS and CdTe); the internal conductance which comprises of convective or series heat transfer coefficient and parallel or radiative heat transfer coefficient, and the thermal resistance which constitutes of convective or series resistance and parallel or radiative resistance are the aftermath of perturbation of the output current and voltage, respectively.

The translation of electrical characteristics into thermal characteristics yielded Tables 8 and 9 which present deterministic (regression) models of the internal conductance and resistance, which are derived from the mechanistic perturbation models in Equations (9) – (26). Lastly, Table 10 shows the comparison of internal conductance for the present work, Churchill and Chu classical correlation, and Engineering Toolbox.

Table 2. Data for crystalline/thin-film semiconductor at AM=1.5 and G=1000 W/m² [1]

S#	Constant /variable	Sym.*	Unit	Crystalline		Thin-film	
				Goldsun JS-SP-Mono-55W [21]	Solarex MSX-60 [22]	Shell solar ST40 [23], [24]	Advanced Solar Power ASP-S4-77 [25]
1.	Semiconductor type	-	-	mono-c-Si	poly-c-Si	CIS	CdTe
2.	Number of cells in series	n_s	-	36	36	42	60
3.	Number of cells in parallel	n_p	-	1	1	1	1
4.	Short circuit current at STC	I_{sc}	A	3.29	3.8	2.68	3.91
5.	Open circuit voltage at STC	V_{oc}	V	21.6	21.1	23.3	28.0
6.	Current at maximum power point	I_{mpp}	A	3.05	3.5	2.41	3.66
7.	Voltage at maximum power point	V_{mpp}	V	18	17.1	16.6	21.0
8.	Temperature coefficient on short circuit current	κ_i	%/K	0.1	0.065	0.035	0.06
9.	Temperature coefficient on open circuit voltage	κ_v	%/K; (%V/K)*	-0.38	-0.08*	-0.10	-0.321
10.	Temperature coefficient on maximum power	κ_p	%/K	-0.47	-5	-0.6	-0.214
11.	Temperature at standard test condition	T_0	K	298.15	298.15	298.15	298.15
12.	Irradiance at standard test condition	G_0	W/m	1000	1000	1000	1000
13.	Boltzmann constant	K_B	J/K	1.3806×10^{-23}	1.3806×10^{-23}	1.3806×10^{-23}	1.3806×10^{-23}
14.	Electron charge	q_c	C	1.6×10^{-19}	1.6×10^{-19}	1.6×10^{-19}	1.6×10^{-19}
15.	Energy gap for thin-film	E_g	eV	1.11	1.11	1.48	1.44
16.	Dimension	L× W× H	(m)	1.675× 0.992× 0.035	1.1082× 0.4668× 0.050	1.264 × 0.643 × 0.035	1.200× 0.600× 0.0068

Sym.* $\Rightarrow$ symbol.

Table 3. Regression of solar irradiance coefficient, γ against temperature coefficient, κ [1]

S#	Semiconductor type	Coefficient	Function	$\overline{\kappa}_i$	$\overline{\gamma}_i$
1	Crystalline: Goldsun JS-SP-Mono-55W (mono-c-Si)	$\kappa_i\,(\%/K)$	$\gamma_i = 0.0814 + 0.2\kappa_i$	0.0770	0.0968
		$\kappa_v\,(\%/K)$	$\gamma_v = 0.0056 + 0.0054\kappa_v$	-0.2510	0.0042
		$\kappa_p\,(\%/K)$	$\gamma_p = 0.013 - 0.3804\kappa_p$	-0.2500	0.1080
2	Crystalline: Solarex MSX-60 (poly-c-Si)	$\kappa_i\,(\%/K)$	$\gamma_i = 0.065 + 1.0\kappa_i$	0.0403	0.1053
		$\kappa_v\,(\%/K)$	$\gamma_v = 0.0032 - 0.0149\kappa_v$	-0.1533	0.0055
		$\kappa_p\,(\%/K)$	$\gamma_p = 0.0112 - 0.3119\kappa_p$	-1.7730	0.5642
3	Thin film: Shell solar ST40 (CIS)	$\kappa_i\,(\%/K)$	$\gamma_i = 0.1562 - 4.8\kappa_i$	0.0227	0.0487
		$\kappa_v\,(\%/K)$	$\gamma_v = 0.0053 - 0.00075\kappa_v$	-0.2693	0.0055
		$\kappa_p\,(\%/K)$	$\gamma_p = 0.0066 - 0.1807\kappa_p$	-0.3510	0.0694
4	Thin film: Advanced Solar Power ASP-S4-77 (CdTe)	$\kappa_i\,(\%/K)$	$\gamma_i = 0.084 + 5\kappa_i$	0.0207	0.1875
		$\kappa_v\,(\%/K)$	$\gamma_v = 0.0007 - 0.025\kappa_v$	-0.2490	0.0069
		$\kappa_p\,(\%/K)$	$\gamma_p = -0.338 - 2.375\kappa_p$	-0.1833	0.0973

Table 4. The computed model parameters at standard condition; 25°C, AM1.5, 1kW/m² [1]

Parameter	Symbol	Unit	Computed value			
			Crystalline semiconductor		Thin-film semiconductor	
			mono-c-Si (Goldsun JS-SP-Mono-55W)	poly-c-Si (Solarex MSX-60)	CIS (Shell solar ST40)	CdTe (Advanced Solar Power ASP-S4-77)
Photon current	I_{ph_0}	A	3.292310	3.805887	2.695131	3.930204
Diode reverse or saturation current	I_{0_0}	A	2.623424×10^{-09}	7.716268×10^{-09}	1.07770×10^{-08}	2.054211×10^{-06}
Ideality factor	A_0	—	1.113246	1.138264	1.289332	1.261012
Shunt or parallel resistance	R_{p_0}	Ω	245.632483	159.295227	70.816000	633.505182
Series resistance	R_{s_0}	Ω	0.173198	0.246767	0.8545173	0.483427

Table 5. The thermophysical properties of air pocket surrounding the semiconductor [1]

S#	Parameter	Unit	Equation
1.	Mean temperature, $\overline{T}$	(K)	
2.	Temperature coefficient, β	(K⁻¹)	$\beta = 1/\overline{T}$
3.	Density, ρ	(kg m⁻³)	$\rho = 2.1313 - 0.003\,\overline{T}$
4.	Viscosity, μ	(kg m⁻¹ s⁻¹)	$\mu = 1.03\times10^{-6} + 7\times10^{-8}\,\overline{T} - 4\times10^{-11}\,\overline{T}^2$
5.	Heat capacity, c_p	(J kg⁻¹ K⁻¹)	$c_p = 1031.31 - 0.0247\,\overline{T} + 0.00042\,\overline{T}^2$
6.	Thermal conductivity, k	(Wm⁻¹ K⁻¹)	$k = 0.0121\exp(0.0025\overline{T})$
7.	Prandtl, Pr	(-)	Equations 29
8.	Rayleigh, Ra	(-)	Equation 29

Table 6. Perturbation of responsive (I and V) with respect to extreme semiconductor temperature (353.15 K)

S#	Semiconductor	Differential (perturbation) operator, $\partial I / \partial T$ (A/K)	Differential (perturbation) operator, $\partial V / \partial T$ (V/K)
1.	Mono crystalline Silicon (mono-c-Si)	0.251717016	0.149909604
2.	Poly crystalline Silicon (poly-c-Si)	0.158307169	0.093463283
3.	Copper indium diselenide, CIS	0.069101490	0.034003935
4.	Cadmium telluride, CdTe	0.085060718	0.044481542

Table 7. Perturbation of responsive (I and V) with respect to diminutive solar irradiance (100 W/m^2)

S#	Semiconductor	Differential (perturbation) operator, $\partial I / \partial G$ (Am^2/W)	Differential (perturbation) operator, $\partial V / \partial G$ (Vm^2/W)
1.	Mono crystalline Silicon (mono-c-Si)	0.004259788	2.736173180
2.	Poly crystalline Silicon (poly-c-Si)	0.005306948	2.771402010
3.	Copper indium diselenide, CIS	0.003440307	1.793220135
4.	Cadmium telluride, CdTe	0.006285375	3.504405002

3.2 Discussion of results

The performance of photovoltaic modules; is obviously influenced by the semiconductor temperature at standard test condition and intensely swayed at the actual operating condition. Thus, the magnitude of the perturbation in Table 6 demonstrates the sensitivity of the individual modules subject to extreme semiconductor temperature. Comparatively, crystalline semiconductors, especially the mono-c-Si depicted the highest magnitude of gradient of the output voltage with respect to extreme semiconductor temperature. This could be attributed to least thermal voltage been developed by the semiconductor as the number of cells in the crystalline modules are less than those of the thin film modules (Table 2).

However, the magnitude of gradient of the output current with respect to extreme semiconductor temperature is higher than that of the output voltage; signifying that more output current is gained as the diode current is being minimised; thus, the diffusion coefficient approaches zero, which implies that the prevailing thermal voltage is higher than the output (electrical) voltage. This phenomenon is analogous to recombination of charge carriers as excess charge carriers are being induced by the extreme semiconductor temperature. Contrarily, Table 7 Portrays the

behaviour of the modules under the diminutive solar irradiance; low gradient of the output current with respect to the diminutive solar irradiance compared to high gradient of the output voltage with respect to the diminutive solar irradiance at actual operating condition, which supports that output voltage is gained at diminutive solar irradiance. The impact of solar irradiance coefficient (Table 3) has significant effect on the analytic equations (Equations (1) – (28)) at diminutive solar irradiance.

Moreover, comparing the gradients of the output current and output voltage in Table 6 indicates that mono-c-Si is the most rugged photovoltaic module at awkward conditions, however, some users are of opinion that its efficiency gradually wanes [26]. Similarly, the thin film semiconductors, especially the CdTe excels under diminutive solar irradiance more than the crystalline semiconductors, this is justified by high gradients both of the output current and output voltage induced by solar irradiance coefficients on the output current and output voltage gradients.

Obviously, Figures 2 and 3 conformed to Karki [7] proposition; with the output current being slightly increased and output voltage appreciably decreased, which results in reduction (or droop) of the output power, which corresponds to the surplus of charge carriers or electron-hole recombination.
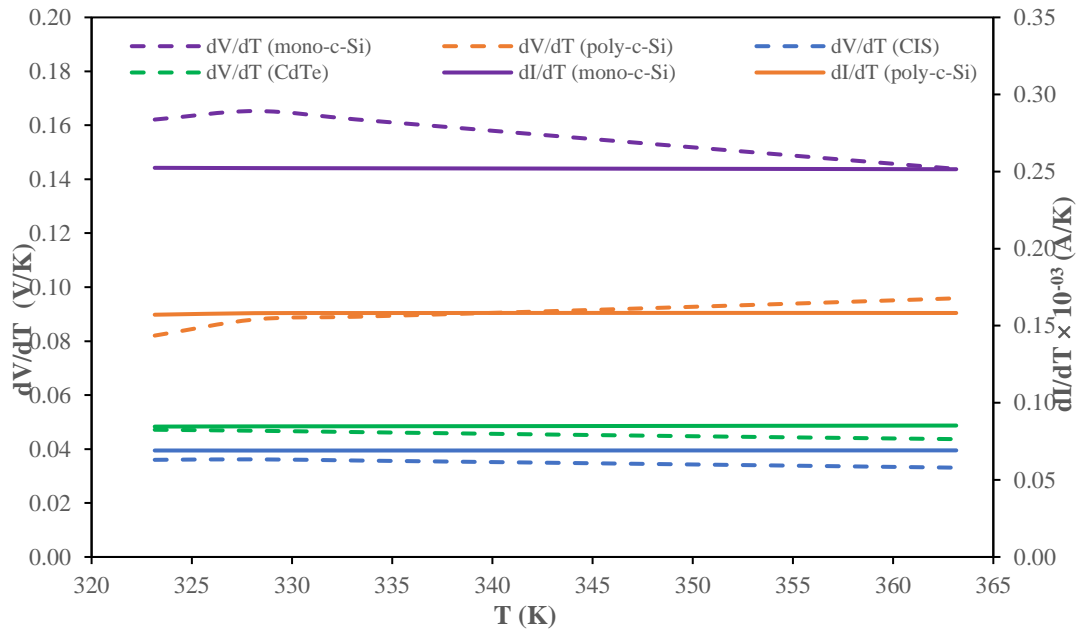
Figure 2. Response of the output current (I) and output voltage (V) to perturbation of semiconductor temperature (T) under diminutive solar irradiance (G ≤ 100 W/m²).

Accordingly, Figure 3 shows that both the output current and voltage increased, leading to appreciation of the output power, which could be attributed to deficit of charge carriers or electron-hole generation, which is in accordance with Sharma et al. [27] findings.

Evidently, the internal conductance of the mono crystalline silicon in Figure 4 is the least compared to other semiconductors, this is sequel to high magnitude of its temperature coefficient on the short circuit current, which diminishes the internal conductance and increases the internal resistance in accordance with Equation (23) and Equation (24), respectively. Also, this phenomenon could have been favoured by high gradients of the output current and output voltage associated with the diminutive solar irradiance and extreme semiconductor temperature in Table 6.

Moreover, the trend of thermal conductance and resistance in Figure 4 is in nonconformity with the general equation of convective heat transfer for liquids; which supports that thermal flux is directly proportional to the product of conductance and temperature difference between the semiconductor and heat transfer fluid.

However, the conductance of air pocket surrounding the semiconductor increases with an increase in the semiconductor temperature whereas its resistance decreases with an increase in the semiconductor temperature; thus, a high semiconductor or air pocket temperature invariably portrays that there is poor ambient or cooling condition (high ambient temperature and low wind speed), which supports the temperature and low wind speed), which supports the recombination of charge

charge carriers whereas low semiconductor or air pocket temperature implies that there is good cooling or ambient condition (low ambient temperature and high wind speed), which favours the generation of charge carriers.

Aptly, Tables 8 and 9 present the effective conductance and resistance as a function of semiconductor temperature. The high regression coefficient which is approximately unity buttress the fact that the models truly represent the thermal conductance and resistance surrounding the semiconductor, which regulates its performance.

Moreover, Table 8 provides an alternative technique for determining the thermal conductance around the semiconductor rather than the tedious technique of assembling series of dimensionless numbers; Nusselt, Grashoff, Prandtl and Rayleigh numbers for determining the internal conductance of fluid pocket surrounding the semiconductors (mono-c-Si, poly-c-Si, CIS and CdTe). This is one of the striking contributions this research has made. Besides, it unveils the dependence of photovoltaic parameters on the stimuli; diminutive solar irradiance and semiconductor temperature.

Furthermore, Table 10 supports the fact that the internal conductance and resistance models developed in the present work (Equations (23) – (28)) are realistic as they compared well with those of Churchill and Chu correlation in [19] and Engineering Toolbox [28] classification for gases.
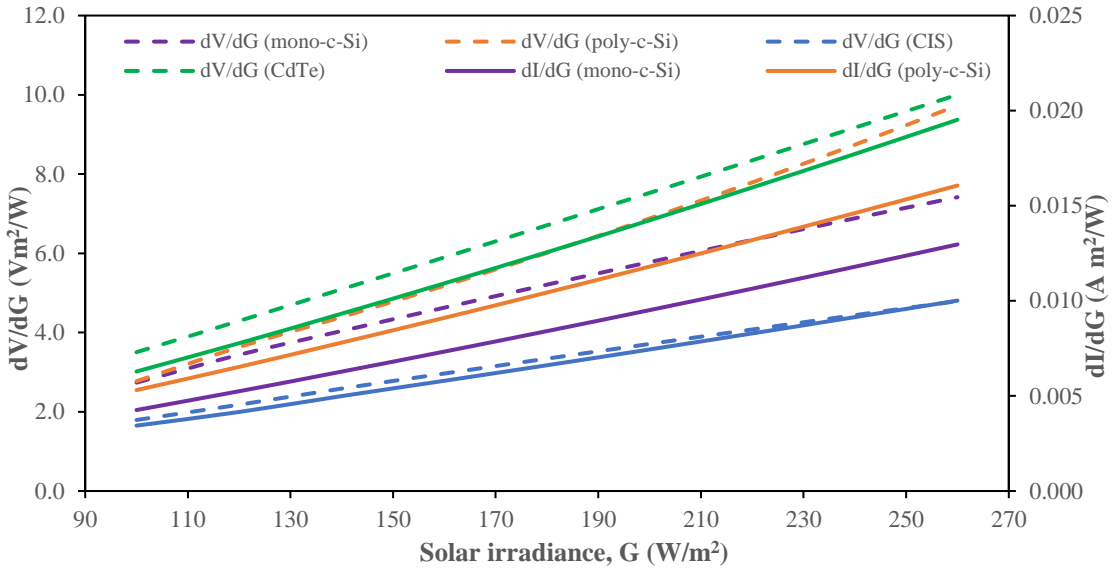
Figure 3. Response of the output current (I) and output voltage (V) to perturbation of solar irradiance (G)
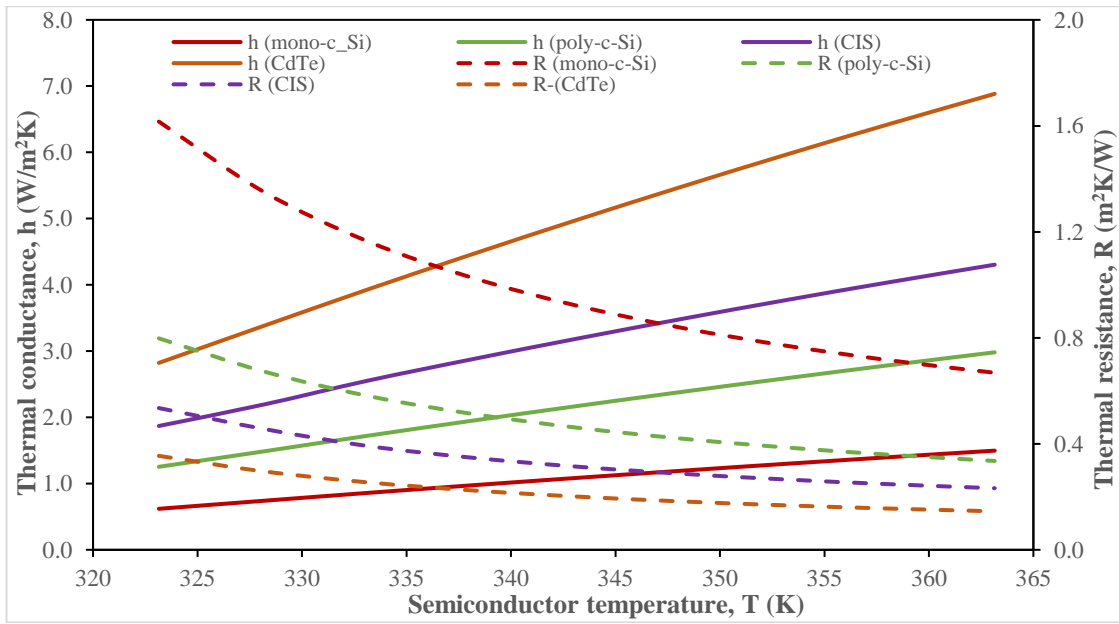

Figure 4. Thermal characteristics of air surrounding the different semiconductors under diminutive solar irradiance (G ≤ 150 W/m²).
under extreme semiconductor temperature (≥ 80 ºC).

Table 8. The internal conductance of air surrounding the semiconductors under a diminutive solar irradiance and extreme semiconductor temperature.

S#	Semiconductor	Effective resistance, $R_{eff} = f(T(K))$ (m²K/ W)	Coefficient of regression, R^2
1.	Mono crystalline Silicon (mono-c-Si)	$R_{eff} = 73.9017802 - 0.4031294\,T + 0.000555\,T^2$	0.9947080
2.	Poly crystalline Silicon (poly-c-Si)	$R_{eff} = 35.5621221 - 0.1936717\,T + 0.0002663\,T^2$	0.9955416
3.	Copper indium diselenide, CIS	$R_{eff} = 23.6149100 - 0.1286484\,T + 0.0001770\,T^2$	0.9956787
4.	Cadmium telluride, CdTe	$R_{eff} = 16.3936749 - 0.0894743\,T + 0.0001232\,T^2$	0.9946869

Table 9. The internal resistance of air surrounding the semiconductors under a diminutive solar irradiance and extreme semiconductor temperature.

S#	Semiconductor	Effective conductance, $h_{eff} = f(T(K))$ (W/m²K)	Coefficient of regression, R^2
1.	Mono crystalline Silicon (mono-c-Si)	$h_{eff} = -6.4593 + 0.0220\,T$	0.9987
2.	Poly crystalline Silicon (poly-c-Si)	$h_{eff} = -12.7130 + 0.0433\,T$	0.9988
3.	Copper indium diselenide, CIS	$h_{eff} = -17.8216 + 0.0611\,T$	0.9976
4.	Cadmium telluride, CdTe	$h_{eff} = -29.9488 + 0.1016\,T$	0.9987

Table 10. Average air internal conductance (W/m²K) for the different semiconductors for the specific conditions; 323.15 ≤ T (ºC) ≤ 363.15 and 100 ≤ G (W/m²) ≤ 260

S#	Semiconductor	Present work	Churchill & Chu correlation [19]	Engineering Toolbox [28] for air, gases and dry vapours
1.	Mono crystalline Silicon (mono-c-Si)	1.090000	6.19885	0.5 – 1000
2.	Poly crystalline Silicon (poly-c-Si)	2.145395	3.68533	0.5 – 1000
3.	Copper indium diselenide, CIS	3.144865	3.63978	0.5 – 1000
4.	Cadmium telluride, CdTe	4.915240	3.65738	0.5 – 1000

4. Conclusion

The perturbation of output current and output voltage with respect to diminutive solar irradiance and extreme semiconductor temperature has been successfully carried out in this work. Consequently, the perturbation of the output current with respect to the stimuli, produced positive stimuli coefficients on the output current, which invariably increased the output current and power. The perturbation of the output voltage with respect to diminutive solar irradiance slightly increased the output voltage sequel to the positive irradiance coefficient on the output voltage whereas with respect to extreme semiconductor temperature depicted a decrease in the output voltage due to negative temperature coefficient on the output voltage.

Relatively, the crystalline modules proved to be more rugged than the thin film modules due to high gradient of the output current (0.085060718 A/K) and output voltage (0.044481542 V/K) with respect to extreme semiconductor temperature whereas the thin film modules overwhelmed the crystalline modules sequel

to high gradient of the output current (0.006285375 Am^2/W) and output voltage (3.504405002 Vm^2/W) with respect to diminutive solar irradiance.

Technically, the perturbation results were translated into the internal conductance and resistance of the heat transfer fluid (air) in contact with the semiconductors, which potentially interpret the cooling mechanism and performance of the semiconductors. Forthwith, a high internal conductance favours surplus of charge carriers and reduction in power generation while a low internal conductance induces deficit of charge carriers and more power generation. Thus, this work has uniquely opened a new technique for evaluating the thermal characteristics of photovoltaic modules from its established electrical characteristics.

References

1. Nnamchi, S.N., et al., *Extrinsic modelling and simulation of helio-photovoltaic system: a case of single diode model.* International Journal of Green Energy, 2019. **16**(6): p. 450-467.

2. Khorasani, A.E., D.K. Schroder, and T.L. Alford, *Principal device engineer at on semiconductor.* IEEE Transactions on Electron Devices, 2014. **35**: p. 986–988.

3. Kirchartz, T., *Generalized detailed balance theory of solar cells.* PhD diss., RWTH Aachen University. Forschungszentrum Jülich Reihe Energie & Umwelt / Energy & Environment Band, 2009. **38**(D 82).

4. Isabella, O., et al., *Solar energy fundamentals, technology, and systems*. 2014: UIT Cambridge.

5. Kant, C.J., *Simulation of quantum dot p-i-n junction solar cell using modified drift diffusion model.* International Journal of Pure and Applied Physics, 2017. **13**(1): p. 59–66.

6. Salim, M.S., J.M. Najim, and S.M. Salih, *Practical evaluation of solar irradiance effect on pv performance.* Energy Science and Technology, 2013. **6**(2): p. 36–40.

7. Karki, I.B., *Effect of temperature on the i-v characteristics of a polycrystalline solar cell.* Journal of Nepal Physical Society, 2015. **3**(1): p. 35–40.

8. Chikate, B.V. and Y.A. Sadawarte, *The factors affecting the performance of solar cell.* International Journal of Computer Applications, 2015: p. 1-5.

9. Ali, M., et al., *Performance investigation of air velocity effects on pv modules under controlled conditions.* International Journal of Photoenergy, 2017. **2017**(3829671): p. 10.

10. Nnamchi, S.N., et al., *Development of dynamic thermal input models for simulation of photovoltaic generators.* International Journal of Ambient Energy, 2018.

11. Cubas, J., S. Pindo, and A. Sanz-Andres, *Accurate simulation of mppt methods performance when applied to commercial photovoltaic panels.* ScientificWorldJournal, 2015. **2015**(914212): p. 16.

12. Hayt, W.H., J.E. Kemmerly, and S.M. Durbin, *Engineering circuit analysis*. 2011: McGraw Hill Higher EducationEnglish. 800.

13. Xie, Y., et al., *Pv system modeling and a global-planning design for its controller parameters*, in *2014 IEEE Applied Power Electronics Conference and Exposition - APEC 2014* 2014, IEEE: Fort Worth Convention Center Fort Worth, TX. p. 3132–3135

14. Ishaque, K., et al., *Modeling and simulation of photovoltaic (PV) system during partial shading based on a two-diode model.* Simulation Modelling Practice and Theory, 2011. **19**(7): p. 1613–1626.

15. Villalva, M.G., J.R. Gazoli, and E. Ruppert, *Modeling and circuit-based simulation of photovoltaic arrays.* Brazilian Journal of Power Electronics, 2009. **14**(1): p. 35–45.

16. Bonkoungou, D., Z. Koalaga, and D. Njomo, *Modelling and simulation of photovoltaic module considering single-diode equivalent circuit model in matlab.* International Journal of Emerging Technology and Advanced Engineering, 2013. **3**(3): p. 493–502.

17. Brano, V.L., A. Orioli, and G. Ciulla, *On the experimental validation of an improved five-parameter model for silicon photovoltaic modules.* Solar Energy Materials & SolarCells, 2012. **105**: p. 27–39.

18. Koch-Ciobotaru, C., et al. *Simulation model developed for a small-scale pv-system in a distribution network.* in *Symposium on Applied Computational Intelligence and Informatics-SACI 2012.* 2012. Timisoara, Romania.

19. Hammami, M., et al., *Thermal and performance analysis of a photovoltaic module with an integrated energy storage system.* Applied Sciences, 2017. **7**(11): p. 1107.

20. Nnamchi, S.N., et al., *Design and fabrication of insulation testing rig.* Indian Journal of Engineering, 2019. **16**: p. 60–79.

21. Goldsun, S. *Js-sp-mono-55w goldsun.* 2018; Available from: https://goldsunsolar.en.made-in-china.com/product/RBSQkDFUOxrT/China-55W-Monocrystalline-Solar-Panel-Cell-Semiconductor.html.

22. Khlifi, Y., *Mathematical modeling and simulation of photovoltaic solar semiconductor in matlab-mathworks environment.* International Journal of Scientific & Engineering Research, 2014. **5**(2): p. 448–454.

23. Shell, S. *Shell st40: thin film cis.* 2018; Available from: http://www.iee.put.poznan.pl/wydawnictwa/wydawnictwaFiles/.pdf.

24. Frydrychowicz–Jastrzębska, G., *CIS, CIGS and CIBS thin film solar cells and possibilities of their application in BIPV.* Computer Applications in Electrical Engineering, 2016. **14**: p. 364-377.

25. Asp, A. *Advanced solar power asp-s4-77.* 2018; Available from: http://www.enfsolar.com/pv/panelhttps://www.enfsolar.com/pv/panel-datasheet/Thinfilm/1022?utm_source=ENF&utm_medium=panel_profile&utm_campaign=enquiry_company_directory&utm_content=2002.

26. *Solar facts and advice.* Available from: http://www.solar-facts-and-advice. com/monocrystalline.html

27. Sharma, A., et al., *Revealing the correlation between charge carrier recombination and extraction in an organic solar cell under varying illumination intensity.* Physical chemistry chemical physics, 2017. **19**(38): p. 26169-26178.

28. Toolbox, E. *Convective heat transfer coefficient.* 2019; Available from: https:www.c.com/convective-heat-transfer-d_430.html.